Nanoscale Horizons

ROYAL SOCIETY OF CHEMISTRY

COMMUNICATION

View Article Online
View Journal | View Issue

Cite this: *Nanoscale Horiz.*, 2025, **10**, 3499

Received 13th July 2025,
Accepted 29th September 2025

DOI: 10.1039/d5nh00488h

rsc.li/nanoscale-horizons

Electrochromic DNA-based bioink with rapid interfacial gelation for bioprinting applications

Yoonbin Ji,[a] Taehyeon Kim,[a] Iksoo Jang[a] and Jong Bum Lee *[ab]

Recent advances in biofabrication demand bioinks that are not only biocompatible and mechanically suitable for tissue engineering, but also responsive to dynamic biological and electrical cues. Here, we introduce a DNA–viologen hybrid bioink system that rapidly forms a structurally defined hydrogel through interfacial gelation, enabling precise spatial control of gelation without requiring external triggers. The resulting hydrogel exhibits a hollow capsule morphology, tunable viscoelasticity, and excellent printability, making it suitable for soft tissue-direct patterning applications. Beyond its mechanical properties, this system integrates reversible electrochromic functionality, allowing dynamic optical responses under electrical stimulation. Taken together, this proof-of-concept study highlights how the integration of electroactive behavior with the programmability of DNA can open opportunities for multifunctional soft materials. The combination of rapid formation, structural adaptability, and electrical responsiveness underscores its promise in emerging applications, including wearable devices, biosensors, and stimuli-responsive platforms.

New concepts

We report a rapidly gelling DNA-based hydrogel ink (RD ink) formed *via* interfacial interaction between DNA and di-*n*-octyl viologen (DOV). Upon contact, DOV was intercalated into DNA strands, triggering immediate gelation and forming hollow structures with tunable shell thickness. AFM and SEM investigations revealed confined, interface-driven gelation and network growth. The DOV–DNA interaction-mediated transient hydrophobic domains served as crosslinking points, forming printable gels with mechanical robustness under repeated strain. Notably, the electrochromic nature of DOV enables reversible color switching of the RD ink under an applied potential, confirmed by cyclic voltammetry and transmittance assays. This system integrated rapid gelation, electrochromic performance, and DNA programmability, presenting a multifunctional material platform for bioelectronic devices, soft actuators, and responsive scaffolds beyond the limits of conventional bioinks.

1. Introduction

Recent advances in biofabrication have increased the demand for hydrogel-based bioinks that can function as tissue-mimicking materials,[1–3] biomedical scaffolds,[4,5] or implantable therapeutic platforms.[6,7] These bioinks require not only controllable gelation kinetics, mechanical fidelity, and biocompatibility, but also precise spatiotemporal control during the printing and curing process to meet the complexity of biological systems. Although various bioinks derived from natural sources—such as alginate, gelatin, and collagen[8–15]—have been widely explored for such purposes, many of them rely on slow physical gelation mechanisms[16] or external stimuli such as light irradiation[17,18] or chemical crosslinkers,[19] which limits their on-site applicability in clinical or *in situ* settings. These limitations highlight the need for next-generation bioink materials that offer both biological compatibility and user-controllable responsiveness without requiring complex external apparatus.

Deoxyribonucleic acid (DNA) has emerged as a promising material for the development of functional materials, owing to its programmability and biocompatibility. Inspired by these advantages, DNA-based hydrogels, which are formed through a three-dimensional network, exhibit inherent biocompatibility, biodegradability, and the potential for structural programmability, making them particularly attractive for applications in tissue engineering,[20–22] drug delivery,[23–25] and cell culture.[26–28] The formation of these DNA hydrogels is commonly achieved through intramolecular or intermolecular hybridization of complementary DNA strands, resulting in networked polymeric structures.[29–31] These hydrogels inherit the polymeric behavior of DNA, enabling them to function as mechanically tunable, elastic, and stimuli-responsive materials.[32–35] Combined with the nanoscale control enabled by nucleic acid design, such systems are uniquely positioned for advanced biomedical applications.

[a] *Department of Chemical Engineering, University of Seoul, 163 Seoulsiripdaero, Dongdaemun-gu, Seoul 02504, Republic of Korea. E-mail: jblee@uos.ac.kr*
[b] *Center for Innovative Chemical Processes, Institute of Engineering, University of Seoul, 163 Seoulsiripdaero, Dongdaemun-gu, Seoul 02504, Republic of Korea*

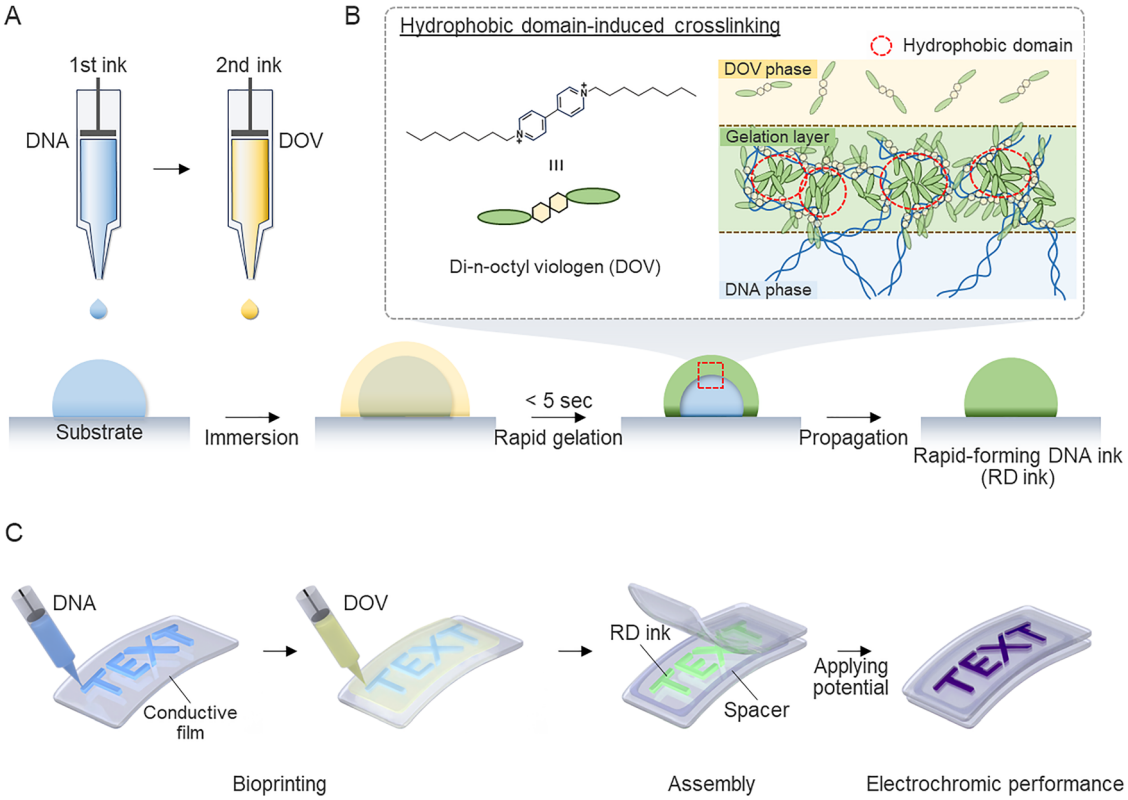

Fig. 1 Fabrication of the rapid forming DNA ink (RD ink) by hydrophobic domain-induced self-assembly. (A) Schematic illustration of (A) the fabrication process of the RD ink and (B) the synthesis mechanism of the hydrophobic domain-mediated gelation process. (C) Electrochromic device fabrication process of the printable RD ink on a desired surface.

In this study, we introduce a rapidly gelling DNA hydrogel system based on 1,1′-di-*n*-octyl-4,4′-bipyridinium dibromide (di octyl viologen, DOV), a viologen derivative that readily interacts with DNA to induce fast gelation (Fig. 1A). Viologens, a class of bipyridinium salts typically represented by the general structure 1,1′-dialkyl-4,4′-bipyridium, have been extensively studied as electrochromic materials due to their distinct color transitions driven by reversible redox transformations.[36–38] The schematic illustration highlights the key mechanisms underlying this system (Fig. 1B). Importantly, viologens also possess planar aromatic rings capable of engaging in π–π stacking interactions with nucleobases,[34,39–43] and their cationic nature enables electrostatic association with the negatively charged phosphate backbone of DNA. These multivalent interactions enable the noncovalent binding of DOV into DNA strands, with a hydrophobic dioctyl carbon chain. The amphiphilic nature of the DNA–DOV strand promotes the formation of hydrophobic intermolecular domains derived from the crowding of adjacent hydrophobic alkyl chains. These domains act as physical crosslinking points that drive the rapid and directional assembly of a hydrogel network (Fig. 1B). By leveraging both the functionality of DNA as a building-block material and the electrochromic properties of DOV, we aim to construct a hybrid material platform suitable as a proof-of-concept for a potential DNA-based bioink (Fig. 1C). This system represents a new direction in the design of printable hydrogels that integrate responsive electroactivity with biomolecular programmability, offering novel possibilities for bioelectronic interfacing applications.

2. Experimental section

2.1. Materials and reagents

DNA sodium salt from salmon testes (dsDNA composed of long strands, >2000 base pairs; D1626), $K_4[Fe(CN)_6]$ (P3289), KCl (793590), $MgCl_2$ (M1028), and ITO-PET (702811) were purchased from Sigma-Aldrich Co. (St. Louis, MO, USA). 1,1′-Di-*n*-octyl-4,4′-bipyridinium dibromide (D1854) was purchased from Tokyo Chemical Industry (Japan). SYBR Green II (S7564) was obtained from Invitrogen (Carlsbad, CA, USA). Fixable Viability Dye eFluor™ and Calcein AM were purchased from Thermo Fisher Scientific (Waltham, MA, USA). Polydimethylsiloxane (PDMS) (SYLGARD 184) was purchased from Sewang Hightech (Republic of Korea). The CCD-986sk (human dermal fibroblast) cell line was purchased from the Korean Cell Line Bank (Seoul, Korea). Dulbecco's modified Eagle's medium (DMEM), fetal bovine serum (FBS), antibiotic–antimycotic (100 ×), penicillin–streptomycin (100×), trypsin-EDTA, and Dulbecco's phosphate-buffered saline (DPBS) were obtained from Gibco (Carlsbad, CA, USA). ITO-coated glass (sheet resistance of 15.0 Ω sq^{-1}) was purchased from Asahi Glass Co. (Japan).

2.2. Fabrication and characterization of RD ink

DNA sodium salt from salmon testes (327 mg) was fully dissolved into 10 mL ultrapure DI water to prepare a DNA solution and 0.5 mmol of 1,1′-di-*n*-octyl-4,4′-bipyridinium dibromide was dissolved in 10 mL of aqueous solution. To fabricate the RD ink, we employed a diffusion-limited interfacial reaction. A droplet of DNA solution was placed onto a hydrophobic substrate or gently added into the DOV solution to react with DOV. Upon contact, rapid gelation occurred exclusively at the DNA–DOV interface, forming a visibly distinct shell within seconds. The sample was incubated for 10 minutes at room temperature to allow further DOV diffusion and shell growth. The resulting hydrogels were gently washed three times with DI water and stored in nuclease-free water at 4 °C prior to further analysis.

2.3. Physical characterization and mechanical testing of the RD ink

The gelation behavior of the DNA–DOV system was monitored by measuring turbidity changes at 600 nm (OD600). DNA and DOV solutions were freshly prepared in ultrapure DI water. 100 μL of each solution was mixed directly in a 96-well transparent plate (SPL) and OD600 was immediately measured using a microplate reader (Synergy HT, BioTek) in kinetic mode. Measurements were taken at 1-second intervals at room temperature. Morphological characterization of the RD ink was performed with field emission scanning electron microscopy (FE-SEM; SU-8010, Hitachi Ltd), followed by freeze-drying. For AFM imaging (Park NX10, Park Systems), each concentration of DNA and DOV solution was dissolved in 10 μL of pH 7.0 TE buffer (IDT) containing 10 mM of $MgCl_2$. The sample was deposited onto a freshly cleaved mica surface and incubated at 4 °C for 15 min. The mica surface was then rinsed with deionized water 3 times to remove salts and dried with nitrogen gas. The sample was scanned in noncontact mode using NC-NCH tips (PPP-NCHR, Park Systems). The viscoelastic properties of the RD ink were analyzed *via* a discovery hybrid rheometer (HR20, TA instruments) with 8 mm parallel plates, while the sample thickness was fixed at ~1 mm.

2.4. Cell Culture and live/dead assay

Human dermal fibroblast cells were grown in DMEM (Gibco) supplemented with 10% fetal bovine serum, 100 units mL^{-1} of penicillin, 100 μg mL^{-1} of streptomycin, and 1% antibiotic–antimycotic at 37 °C in a humidified atmosphere supplemented with 5% CO_2. A density of 40 000 cells mL^{-1} was seeded in a 24 well culture plate. 24 hours after seeding, the medium was exchanged with reduced serum medium and each amount of RD ink was added to each well. After 24 h incubation, the cells were washed with DPBS and stained with Fixable Viability Dye eFluor™ and Calcein AM following the manufacturer's instructions. To quantify the viable cells, the fluorescence signal of the harvested cells at each time point was measured by a Nucleocounter (NC-3000, Chemometec, Denmark).

2.5. Electrochemical properties of the RD ink

To adjust the lower EC operation voltage, 5 mM $K_4[Fe(CN)_6]$ and 100 mM KCl were used as the anodic species and electrolyte, respectively. The fabricated RD ink was immersed in the prepared electrolyte for 15 min to achieve anodic substitutions. The electrochemical properties of the RD ink were analyzed using a ZIVE SP1 electrochemical workstation (WonATech, Korea). Similarly, for observation of coloration, the output bias was applied using a potentiostat (Wave Driver 10, Pine Instrument).

3. Results and discussion

3.1. Fabrication and characterization of the rapid forming DNA ink (RD ink)

To induce the rapid gelation at the DNA-DOV interface, we introduced the DNA solutions, either dispensed as droplets or precast into desired shapes, and subsequently exposed the solution to the DOV solution. Upon contact, the DNA phase immediately underwent interfacial complexation with DOV, leading to the formation of the crosslinked hydrogel. By dripping the DNA solution into DOV solution, rapid gelation proceeded immediately from the interface, resulting in a spherical structure with well-defined boundaries to construct the rapid-forming DNA ink (RD ink) (Fig. 2A, Video S1). This spatiotemporally controllable gelation process was visualized by tracking the fluorescence of SYBR green II-stained DNA over time. During the rapid gelation, the DNA-intercalating fluorescence probe was trapped in the crosslinked hydrogel within 5 s (Fig. S1). Optical density (OD) measurement was used to monitor the turbidity which associated with DOV-induced network formation. It confirmed the triggered gelation of the DOV-induced network formation, OD change was not detected for low concentrations of DOV and this suggested that critical concentration for bulk gelation (Fig. 2B). The products from diverse ratios of DNA:DOV presented partially gelated solutions below the critical concentration ratio between DNA and DOV (Fig. S2). As shown in Fig. 2C, the fluorescence signal diminished progressively from the outer surface toward the core, suggesting directional gelation from the interface. This signal loss is attributed to competitive displacement of the intercalated dye by DOV molecules during network formation (Fig. S3). Moreover, AFM analysis of the diluted DNA–DOV mixtures revealed the formation of progressively larger DNA aggregates as the DOV concentration increased (Fig. 2D and Fig S4). These aggregates were likely to serve as nucleation centers for the macroscopic network structure. From these results, we suggest that the interface-confined gelation proceeds *via* a diffusion-mediated mechanism, initiated by the aggregation of the DNA–DOV complexes formed by multivalent interactions of DNA and DOV. In Fig. 2E, the SEM images of the cross-sectioned formed hydrogels revealed a hollow capsule structure, with a distinct shell thickness dependent on the DNA and DOV ratio (Fig. 2F). Thicker shells were observed at higher DOV concentrations, consistent with the increased network density observed in AFM

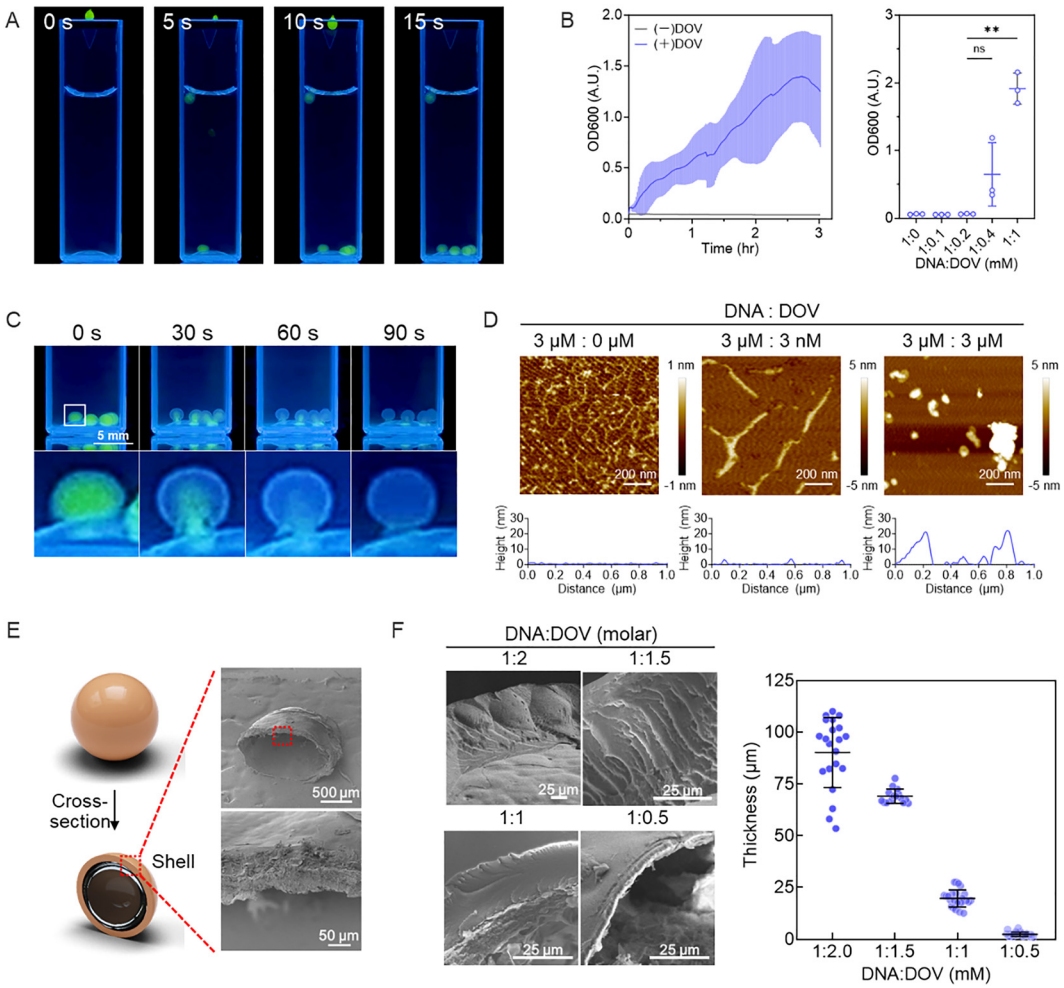

Fig. 2 Rapid gelation of the RD ink and characterization. (A) Snapshot images of the fabrication process of the RD ink. SYBR Green II stained DNA solution was dropped into DOV solution. Digital images were taken under UV irradiation. (B) Optical property change on the gelation process. OD600 of the RD ink was measured over time and at each concentration ratio of DNA:DOV. (C) Digital images of the RD ink after gelation. Images were taken under UV irradiation. (D) AFM analysis of the reacted DNA with each molar concentration of DOV. The line profile is indicated by the dashed lines on each image. (E) FE-SEM images of the cross-sectioned RD ink (top) and magnified image of the white dashed box (bottom). (F) SEM images of the RD ink formed from different molar ratios between DNA and DOV. The thickness of each hollow structure was measured by imageJ software.

analysis. To evaluate the potential cytotoxicity in proposed practical applications, such as direct contact with the skin surface or in a separated wearable device, preliminary cell viability assays were performed at different concentrations of RD ink. As shown in Fig. S5, concentrations below 2 mg ml^{-1} of DNA showed no detectable cytotoxic effects, while an indirect co-culture assay using a transwell system revealed lower and delayed cytotoxicity compared to direct contact (Fig. S6). These results indicate that the RD ink could be suitable in situations where systemic exposure is limited, as long as surface interactions are carefully managed.

3.2. Mechanical properties and spatial patterning capability

The mechanical properties of the RD ink were characterized to evaluate its suitability for extrusion-based bioprinting applications. Upon exposure of DOV into the DNA solution, both the storage (G') and loss (G'') moduli rapidly increased from 70 Pa to 190 Pa, indicating the triggered gelation (Fig. 3A). Triggered gelation could also realize the desired pattern by immersing the precast DNA solution onto DOV solution, as shown in Fig. 3B. The RD ink exhibited a modulus range of about hundreds of Pa, which lies within the optimal range for soft tissue-mimicking applications.[44–46] Strain sweep analysis revealed the viscoelastic behavior of the gel across a wide deformation window, with stable G′ values maintained up to ∼10% strain and a rapid drop-off at higher deformations (Fig. 3C). Frequency sweep data confirmed that $G' > G''$ across the relevant dynamic range (1–100 rad s^{-1}), further supporting gel-like behavior (Fig. 3D). Under alternating large and small strain (1% ↔ 500%), the hydrogel exhibited partial recovery of the modulus after the first cycle and stable performance over six cycles (Fig. 3E), indicating mechanical recovery and suitable for printability under repeated stress. Moreover, the rheological properties could be tuned by the structural features of the hollow architecture, which is shown in Fig. F2. By adjusting the ratio between DNA and DOV, both the storage and loss modulus of

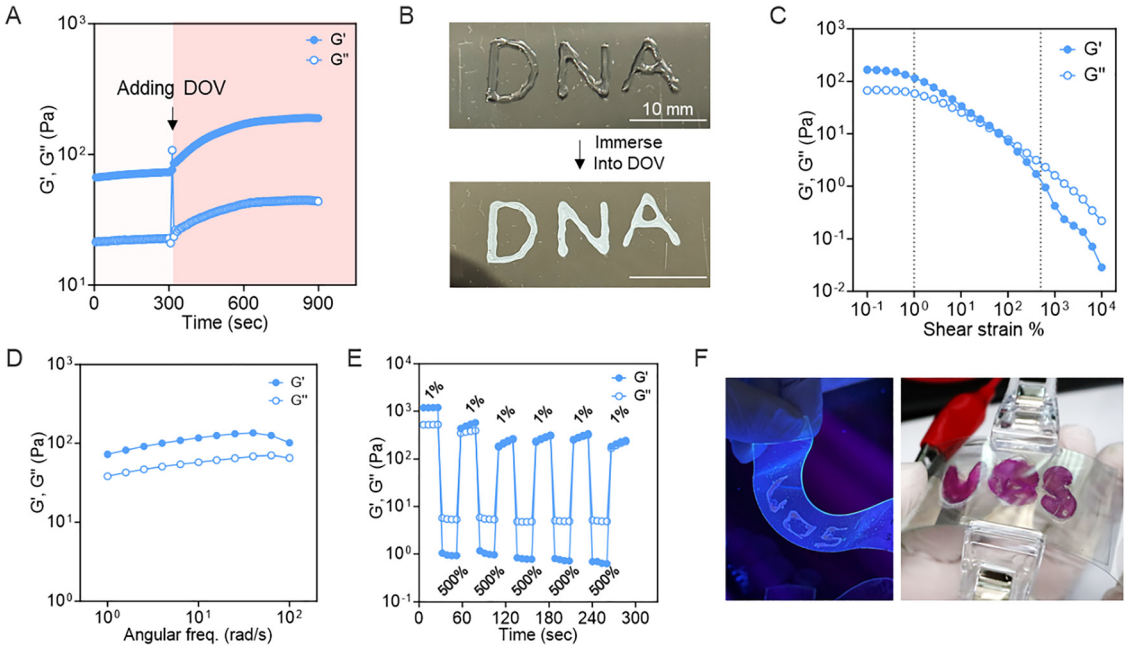

Fig. 3 Mechanical properties and printability of the RD ink. (A) Rheological test during the gelation process of the RD ink. DOV solution was added into DNA solution during the measurement. (B) Representative images of the on-site gelation process of the RD ink. Pre-printed DNA solution underwent a gelation process after DOV treatment. (C) Viscoelastic properties of the RD ink on strain sweep analysis in the range of 10^{-1}% to 10^{4}% of shear strain. (D) Frequency sweep test across the range of angular frequency. (E) The changing storage/loss modulus of the RD ink in alternating strain tests between low strain (1%) and high strain (500%). (F) Representative digital image of the prepared RD ink on a flexible PET film surface with the desired shape, stained with GelRed (left) and RD ink after coloration (right).

RD ink were increased with greater shell thickness increases (Fig. S7). This suggests that the mechanical properties of the RD ink can be tailored through compositional design, enabling optimization for diverse printing conditions. With these results, RD ink could be printed on the desired surface, including flexible polymeric films (Fig. 3F and Video S2).

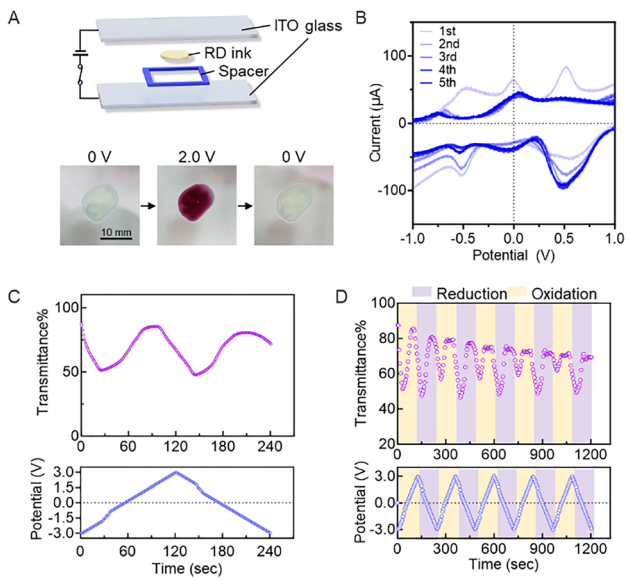

Fig. 4 Electrochromic behavior of the RD ink. (A) Schematic illustration of the design of the RD ink-based electrochromic device and representative image of the coloration of the RD ink with an applied potential. (B) Electrochemical properties of the RD ink in repeated testing of cyclic voltammetry. (C) Transmittance change of a 532 nm laser irradiated through the RD ink with an applied potential. (D) Transmittance change on cyclic potential test.

3.3. Electrochromic functionality of the RD ink

In addition to mechanical robustness and printable characteristics, the RD ink system exhibited distinct electrochromic behavior. When sandwiched between two ITO electrodes and a voltage was applied, the initial colorless gel became visibly purple (Fig. 4A). This color change was reversible and corresponded with redox transitions confirmed by cyclic voltammetry (Fig. 4B). The anodic peak observed in the first cycle can be ascribed to a transient break-in effect at the unconditioned ITO–hydrogel interface, after which the formation of a stable hydroxyl layer leads to more uniform interfacial behavior.[47–49] The transmittance of a 532 nm laser beam through the hydrogel film decreased significantly during coloration and recovered on restoration of the potential (Fig. 4C), suggesting potential use in optoelectronic or sensing applications. Notably, this coloration–bleaching behavior remained stable under repeated voltage cycling (Fig. 4D), underscoring the durability of the RD ink as an electrochromic hydrogel and its potential utility in soft optoelectronic applications.

Conclusions

In this study, we introduced a novel crosslinked hydrogel system based on the rapid interfacial gelation of DNA with viologen molecules. This system enables instantaneous and

spatially controlled hydrogel formation without external triggers such as light or heat, addressing limitations of conventional biomaterial-based bioinks. The structural propagation of the hydrogel, from molecular level aggregation to macroscopic hollow capsule formation, was systematically characterized, revealing a controllable and interface-driven gelation mechanism. Mechanical property investigations confirmed that the gel possessed suitable viscoelastic properties for soft biomedical interfaces and repeated stress cycles, ensuring potential in bioprinting and *in situ* gelation. In addition, the electrochromic performance of the RD ink under an applied potential highlights its utility as a functional material capable of dynamic coloration on-demand interfacing. Together, the integration of programmable DNA structures with redox-responsive viologens presents a promising strategy for designing next-generation, multifunctional bioinks. This platform not only enables rapid and precise gelation but also offers pathways for optical sensing. At this stage, the system is mainly practically envisioned for applications such as wearable electrochromic devices or *ex vivo* biosensing assays, while still having potential for broader biomedical integration pending further optimization.

Author contributions

Yoonbin Ji: conceptualization, methodology, investigation, and writing, Taehyeon Kim: investigation and formal analysis, Iksoo Jang: fabricating ECD device and formal characterization and Jong Bum Lee: supervision and editing.

Conflicts of interest

The authors declare no competing interests.

Data availability

Data for this article, including additional figures are available at **https://doi.org/10.1039/d5nh00488h**.

Acknowledgements

This research was supported by the National Research Foundation of Korea (NRF) grants funded by MSIT [RS-2022-NR070138], [RS-2025-02217898] and by a grant from the Korea Health Technology R&D Project through the Korea Health Industry Development Institute (KHIDI), funded by the Ministry of Health & Welfare [RS-2024-00437312].

Notes and references

1 M. Samandari, J. Quint, A. Rodríguez-delaRosa, I. Sinha, O. Pourquié and A. Tamayol, *Adv. Mater.*, 2022, **34**, 2105883.
2 S. Ji and M. Guvendiren, *Front. Bioeng. Biotechnol.*, 2017, **5**, DOI: **10.3389/fbioe.2017.00023**.
3 A. Skardal, M. Devarasetty, H.-W. Kang, I. Mead, C. Bishop, T. Shupe, S. J. Lee, J. Jackson, J. Yoo, S. Soker and A. Atala, *Acta Biomater.*, 2015, **25**, 24–34.
4 D. Gogoi, M. Kumar and J. Singh, *Annals 3D Printed Medicine*, 2024, **15**, 100159.
5 Y. Luo, G. Luo, M. Gelinsky, P. Huang and C. Ruan, *Mater. Lett.*, 2017, **189**, 295–298.
6 C. W. Peak, K. A. Singh, M. Adlouni, J. Chen and A. K. Gaharwar, *Adv. Healthcare Mater.*, 2019, **8**, 1801553.
7 G. Gao, J. H. Lee, J. Jang, D. H. Lee, J.-S. Kong, B. S. Kim, Y.-J. Choi, W. B. Jang, Y. J. Hong, S.-M. Kwon and D.-W. Cho, *Adv. Funct. Mater.*, 2017, **27**, 1700798.
8 S. Debnath, A. Agrawal, N. Jain, K. Chatterjee and D. J. Player, *J. Mater. Chem. B*, 2025, DOI: **10.1039/D4TB01060D**.
9 S. Asim, T. A. Tabish, U. Liaqat, I. T. Ozbolat and M. Rizwan, *Adv. Healthcare Mater.*, 2023, **12**, 2203148.
10 Y. P. Singh, A. Bandyopadhyay and B. B. Mandal, *ACS Appl. Mater. Interfaces*, 2019, **11**, 33684–33696.
11 T. Gao, G. J. Gillispie, J. S. Copus, A. K. PR, Y.-J. Seol, A. Atala, J. J. Yoo and S. J. Lee, *Biofabrication*, 2018, **10**, 034106.
12 S. Bertlein, G. Brown, K. S. Lim, T. Jungst, T. Boeck, T. Blunk, J. Tessmar, G. J. Hooper, T. B. F. Woodfield and J. Groll, *Adv. Mater.*, 2017, **29**, 1703404.
13 E. Axpe and M. L. Oyen, *Int. J. Mol. Sci.*, 2016, **17**, 1976.
14 P. Rastogi and B. Kandasubramanian, *Biofabrication*, 2019, **11**, 042001.
15 K. Markstedt, A. Mantas, I. Tournier, H. Martínez Ávila, D. Hägg and P. Gatenholm, *Biomacromolecules*, 2015, **16**, 1489–1496.
16 A. Skardal, J. Zhang, L. McCoard, S. Oottamasathien and G. D. Prestwich, *Adv. Mater.*, 2010, **22**, 4736–4740.
17 S. Knowlton, B. Yenilmez, S. Anand and S. Tasoglu, *Bioprinting*, 2017, **5**, 10–18.
18 L. E. Bertassoni, J. C. Cardoso, V. Manoharan, A. L. Cristino, N. S. Bhise, W. A. Araujo, P. Zorlutuna, N. E. Vrana, A. M. Ghaemmaghami, M. R. Dokmeci and A. Khademhosseini, *Biofabrication*, 2014, **6**, 024105.
19 Y. Zhang, Y. Yu, A. Akkouch, A. Dababneh, F. Dolati and I. T. Ozbolat, *Biomater. Sci.*, 2014, **3**, 134–143.
20 C. Chen, J. Zhou, J. Chen and H. Liu, *Macromol. Biosci.*, 2022, **22**, 2200152.
21 A. Gangrade, N. Stephanopoulos and D. Bhatia, *Nanoscale*, 2021, **13**, 16834–16846.
22 L. D. Shea, E. Smiley, J. Bonadio and D. J. Mooney, *Nat. Biotechnol.*, 1999, **17**, 551–554.
23 S. Han, Y. Park, H. Kim, H. Nam, O. Ko and J. B. Lee, *ACS Appl. Mater. Interfaces*, 2020, **12**, 55554–55563.
24 O. Ko, S. Han and J. B. Lee, *J. Ind. Eng. Chem.*, 2020, **84**, 46–51.
25 D. Kim, H. Kim, P. C. W. Lee and J. B. Lee, *Mater. Horiz.*, 2020, **7**, 1317–1326.
26 H. Nam, H. Jeon, H. Kim, H. Y. Yoon, S. H. Kim and J. B. Lee, *Chem. Eng. J.*, 2023, **452**, 139492.
27 J. Wu, B. R. Liyarita, H. Zhu, M. Liu, X. Hu and F. Shao, *ACS Appl. Mater. Interfaces*, 2021, **13**, 49705–49712.
28 A. Finke, A.-K. Schneider, A.-S. Spreng, M. Leist, C. M. Niemeyer and A. Marx, *Adv. Healthcare Mater.*, 2019, **8**, 1900080.

29 J. Gačanin, C. V. Synatschke and T. Weil, *Adv. Funct. Mater.*, 2020, **30**, 1906253.
30 F. Huang, M. Chen, Z. Zhou, R. Duan, F. Xia and I. Willner, *Nat. Commun.*, 2021, **12**, 2364.
31 J. B. Lee, S. Peng, D. Yang, Y. H. Roh, H. Funabashi, N. Park, E. J. Rice, L. Chen, R. Long, M. Wu and D. Luo, *Nat. Nanotech.*, 2012, **7**, 816–820.
32 Y. Hu and J. Y. Ying, *Materials Today*, 2023, **63**, 188–209.
33 S. Iqbal, F. Ahmed and H. Xiong, *Chem. Eng. J.*, 2021, **420**, 130384.
34 Y. Ji, T. Kim, D. Han and J. B. Lee, *ACS Materials Lett.*, 2024, **6**, 1277–1287.
35 C. Wang, X. Liu, V. Wulf, M. Vázquez-González, M. Fadeev and I. Willner, *ACS Nano*, 2019, **13**, 3424–3433.
36 K. Madasamy, D. Velayutham, V. Suryanarayanan, M. Kathiresan and K.-C. Ho, *J. Mater. Chem. C*, 2019, **7**, 4622–4637.
37 D. Liang, Z. Guo, Y. Su, F. Zhou, M. Wang, W. Chen and G. Zhou, *Adv. Mater. Technol.*, 2023, **8**, 2300454.
38 Z. Tajmoradi, H. Roghani-Mamaqani, K. Asadpour-Zeynali and M. Salami-Kalajahi, *Microchem. J.*, 2024, **207**, 111698.
39 H. Jeon, Y. M. Kim, S. Han, H. C. Moon and J. B. Lee, *ACS Nano*, 2022, **16**, 241–250.
40 S. K. Saraswathi, V. Karunakaran, K. K. Maiti and J. Joseph, *Front. Chem.*, 2021, **9**, 716–771.
41 S. N. Topkaya, A. Karasakal, A. E. Cetin, S. Parlar and V. Alptüzün, *Electroanalysis*, 2020, **32**, 1780–1787.
42 T. Kakibe and H. Ohno, *Chem. Commun.*, 2008, 377–379.
43 S. Takenaka, H. Sato, T. Ihara and M. Takagi, *J. Heterocycl. Chem.*, 1997, **34**, 123–127.
44 V. R. Feig, H. Tran, M. Lee and Z. Bao, *Nat. Commun.*, 2018, **9**, 2740.
45 S. Gong, L. W. Yap, B. Zhu and W. Cheng, *Adv. Mater.*, 2020, **32**, 1902278.
46 L. Zhang, K. S. Kumar, H. He, C. J. Cai, X. He, H. Gao, S. Yue, C. Li, R. C.-S. Seet, H. Ren and J. Ouyang, *Nat. Commun.*, 2020, **11**, 4683.
47 E. Matveeva, *J. Electrochem. Soc.*, 2005, **152**, H138.
48 P. M. M. C. Bressers and E. A. Meulenkamp, *J. Electrochem. Soc.*, 1998, **145**, 2225.
49 X. Song, H. Yan, Y. Zhang, W. Zhou, S. Li, J. Zhang, S. Ciampi and L. Zhang, *Chem. Commun.*, 2024, **60**, 4186–4189.